Visible and Near-Infrared Properties of Optical Fibers Coupled to the Pathfinder High-Resolution NIR Spectrograph

Keegan S. McCoy
Department of Electrical Engineering and Department of Astronomy and Astrophysics
Pennsylvania State University, University Park, PA
ksm5052@psu.edu

Larry W. Ramsey
Department of Astronomy and Astrophysics
Pennsylvania State University, University Park, PA

ABSTRACT

The Penn State Astronomy and Astrophysics Department's Pathfinder instrument is a fiber-fed, warm-bench echelle spectrograph designed to explore technical issues that must be resolved in order to measure precise radial velocities that will allow the detection of exoplanets in the near-infrared (NIR). In May 2010, Pathfinder demonstrated 10-20 m/s radial-velocity precision in the NIR at the 9 meter Hobby-Eberly Telescope. To attain even higher precision, we are investigating the NIR properties of the optical fibers that transmit light from the telescope to Pathfinder. We conducted a series of modal noise tests with visible and NIR laser diodes on a 200 micron diameter, fused-silica, multimode optical fiber as the preliminary step in analyzing the degrading effects of modal noise on radial-velocity precision. We report these test results and comment on our future tests to reduce the negative effects of modal noise and focal ratio degradation (FRD). The lessons learned from this research and the Pathfinder prototype will be used in Pathfinder II, which will aim to achieve better than 5 m/s in the NIR.

1. INTRODUCTION

The search for exoplanets, particularly those that may be habitable, is currently one of the fastest-growing fields of astronomical research. M dwarfs, the most common stellar classification, comprise at least 70% of the stars in our Milky Way Galaxy. Therefore, detecting and determining the habitability of M dwarfs provides us with a lower limit on the habitability of the Milky Way and the universe in general. M dwarfs range in mass from about 0.075 to 0.40 solar masses and have temperatures between 2,500 K and 3,500 K. This means that the peak of an M dwarf's spectrum is in the near-infrared (NIR).

The most successful means of detecting exoplanets has been the radial-velocity method, by which Doppler shifts of absorption lines in a host star's spectrum can be used to determine the number of planets orbiting the star, along with the planetary masses and orbital distances. The mutual gravitational attraction of the star and its planets introduces a relatively small, but detectable "wobble" in the host star's motion, as both the star and planets orbit around the common barycenter of the system. A majority of the 598 exoplanets discovered to date [1] have been found using the radial-velocity method at visible wavelengths, detecting Jupiter- or Neptune-mass planets orbiting solar-mass stars. However, M dwarfs offer the opportunity to discover Earth-mass, potentially habitable planets, since the mass ratio between an Earth-mass planet and an M dwarf is much greater than for an Earth-mass planet and a solar-mass star. The higher relative gravitational attraction between an M dwarf and an Earth-mass planet therefore produces a much more noticeable radial-velocity signature on an M dwarf's spectrum than it would for a solar-mass star. Due to the low mass of M dwarfs and the close range of their habitable zones, about 0.02 to 0.3 Astronomical Units (AU), radial-velocity amplitudes of M dwarf habitable zone planets will be on the order of 1 m/s [2]. If Earth-mass M dwarf exoplanets are detected in the habitable zone of their host stars, defined as the orbital distance at which liquid water can exist on the planet's surface [3], they may possibly harbor life. Before that exciting prospect can be fully realized, however, engineers and astronomers face many challenges in designing high-precision exoplanet-detection systems.

2. MODAL NOISE

From electromagnetic theory, it is known that electromagnetic waves propagate through a waveguide in a specified set of modes that depends on the wavelength of the propagating radiation and the waveguide's boundary conditions. Nevertheless, a simple ray model is useful in conceptualizing modal propagation through optical fibers. Fig. 1 displays a geometrical representation of modes propagating through a multimode optical fiber, with the fundamental mode entering the fiber input face on-axis and higher order modes entering at increasing angles up to the fiber's numerical aperture. It can be seen that coherent light entering a fiber within a particular angular range (or focal ratio) will excite a unique set of modes and produce a specified modal power distribution (MPD). Each mode has a different propagation constant, β, meaning that every mode travels a different distance in a given time interval. These modes present themselves as a speckle pattern in the fiber's far field. A change in the input illumination of a fiber therefore alters the far-field speckle pattern and the fiber's MPD.

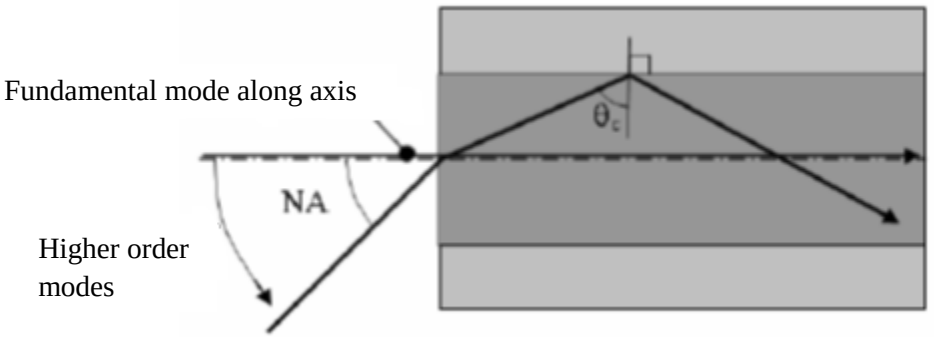

Fig. 1. Modal propagation through an optical fiber [4]

Non-uniformities in a fiber, such as index of refraction variations, fiber diameter variations, core-cladding interface irregularities, and core scattering centers affect modal propagation in a quasi-random manner, redistributing power between the various modes. In addition to these internal factors, external stresses, temperature fluctuations, and beam truncation also change the modal distribution in a fiber. An example of these effects is shown in Fig. 2, once again using the ray model for mode propagation. Light is scattered into a given mode from many different modes, so that when the light reaches the fiber end face, it exhibits a quasi-random phase and amplitude variation in the resulting far-field speckle pattern [4]. Light entering a perfect fiber with no irregularities will exit with the same modal distribution and focal ratio. However, in the real world higher order modes than what originally entered the fiber will inevitably be excited through this redistribution of modal power. Hence, fibers have the tendency to decrease the focal ratio of input light, i.e. light will exit a fiber within a larger angular cone than when it entered the fiber, an effect known as focal ratio degradation (FRD). FRD reduces the throughout efficiency and resolution of a spectrograph.

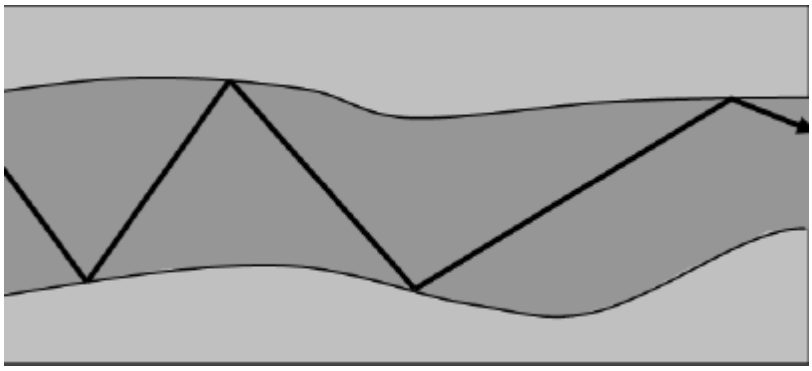

Fig. 2. Effect of fiber non-uniformity on modal propagation [4]

Modal noise, the time variation of the MPD, is of particular concern when measuring precise radial velocities, since the stability of the instrument profile on the spectrograph is key in measuring the tiny Doppler shifts induced by

exoplanets on their host stars. Optical fibers provide better illumination stability for a spectrograph than simply an aperture or slit, since fibers smooth out seeing and guiding variations due to their modal scrambling characteristics [5]. Fibers are particularly good at scrambling light azimuthally, though radial scrambling is not complete, retaining some information of the fiber's input illumination. Nevertheless, optical aberrations in instrument optics and fiber imperfections can cause radial-velocity shifts greater than 1 m/s [6]. Mechanical agitators and optical scramblers can be used to increase fiber scrambling ability and reduce any dependency on variable illumination conditions.

The number of excited modes in a fiber is given by eq. (1):

$$M = \frac{1}{2} \cdot \left(a \cdot \frac{2\pi}{\lambda} \cdot \theta \right)^2 \quad (1)$$

where a is the fiber core radius, λ is the light's wavelength, and θ is the fiber coupling angle. Eq. (2) [7] demonstrates the relationship between the number of modes in a fiber and the corresponding signal to noise ratio:

$$SNR = \rho^2 \cdot \sqrt{\frac{M+1}{1-\rho^2}} \quad (2)$$

with vignetting factor $\rho^2 = A_d / A_f$; A_f is the illuminated area of the fiber end face and A_d the effective detector area illuminated by the fiber. Substituting eq. (1) into eq. (2), it is clear that *SNR* decreases inversely proportional with λ. Consequently, reduction of *SNR* is more significant at longer wavelengths, so understanding and mitigating modal noise is even more crucial in the NIR.

3. LASER DIODE MODAL NOISE TESTS

The following tests represent a preliminary step in characterizing and mitigating modal noise in Penn State's Pathfinder spectrograph. Though more extensive FRD and modal noise tests will soon follow, these early tests provide a glimpse into the experimental subtleties of measuring modal noise in the visible and NIR. For these experiments, modal noise was measured at 635 nm and 1550 nm using Thor Labs laser diodes, which are pigtailed to 1 meter long single mode fibers with an FC/PC connector. Table 1 provides the specifications for these laser diodes, along with the currents and voltages used in testing.

Table 1. Thor Labs laser diodes used in modal noise testing

	LPS-635-FC	LPS-1550-FC
Wavelength	635 nm	1550 nm
Output Power	2.5 mW	1.5 mW
Test Current	57.3 mA	21.8 mA
Test Voltage	2.252 V	0.969 V

For all tests, a Thor Labs ITC 4001 Laser Diode/Temperature Controller was used to set the laser diode currents and keep the diode temperatures stable at 23 °C. The 635 nm and 1550 nm laser diodes were alternately coupled to an Edmund Optics 1 meter 0.22 NA VIS/NIR patchcord 200 micron multimode fiber (NT57-748) with an FC connector. Using this setup, it is known that the input to the multimode fiber is only the single fundamental mode of coherent laser light at the given laser diode's wavelength. Therefore, any resulting modal noise detected on the multimode fiber's output face will be solely due to the multimode fiber's irregularities. The multimode fiber was then mounted and the light collimated so that it could be detected on a Xenics Xeva-1.7-320 NIR camera, which has a 256 x 320 pixel array with peak sensitivity from 900-1700 nm (< 30% QE at 635 nm and 84% QE at 155 nm). A Newport motorized iris (Model 62280) was used to reduce the collimated beam diameter so that it fit on the NIR camera's detector. An FMC Syntron PowerPulse electromagnetic vibrator was used to vibrate the multimode fiber at 60 Hz, so that static and vibrated results could be compared for 635 nm and 1550 nm. Fig. 3 shows the entire test setup, while Fig. 4 focuses in on the vibrator.

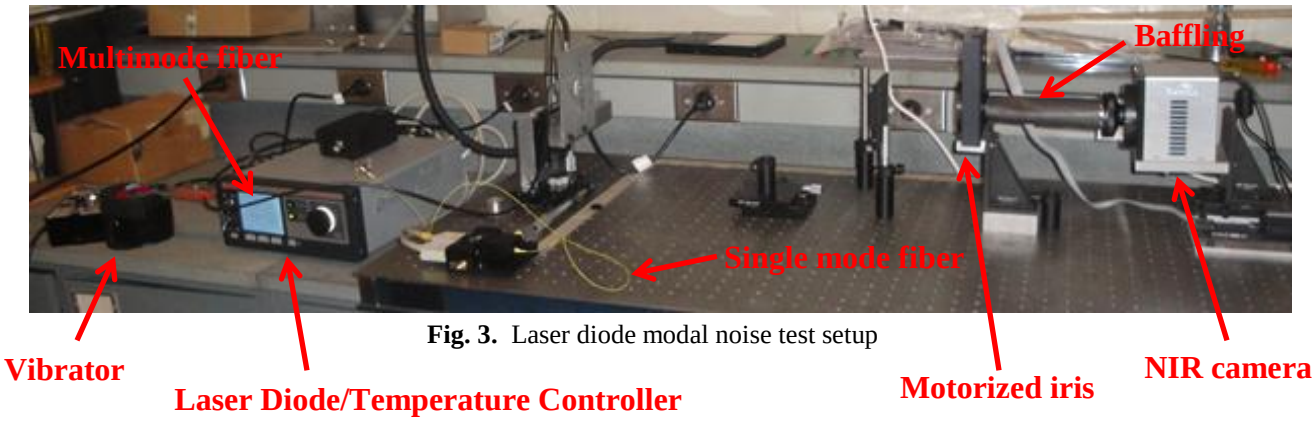

Fig. 3. Laser diode modal noise test setup

Fig. 4. Vibrator attached to 200 micron multimode fiber

Flat field frames were taken by placing a Dolan-Jenner Fiber-Lite area backlight in front of the motorized iris and opening the motorized iris 100% (36 mm diameter). For the laser diode tests, the motorized iris was set to 5% open (3.7 mm diameter), while both neutral density filers were used and frame integration times were adjusted to limit the maximum counts to roughly half of the NIR camera detector's dynamic range. Frames were also taken of just the 635 nm single mode fiber without the multimode fiber connected to compare to the multimode results. Table 2 summarizes the test procedure and Fig. 5 shows a 635 nm static test in progress.

For each test listed in Table 2, 10 sets of frames were taken, with each set consisting of 10 frames taken in sequence. Individual sets were taken 1 minute apart to provide significant temporal separation over the course of all 10 sets. For the static tests, the multimode fiber was flicked once between individual sets to mix the modes. The vibrator was vibrated at 60 Hz for all 10 vibrated sets taken for the 635 nm and 1550 nm laser diodes. The vibrator has a 10-pt. amplitude scale, so 4 sets were taken at amplitude level 4, 3 sets at amplitude level 3 and 3 sets at amplitude level 2. The test order of the vibration amplitude levels was randomized for all 10 sets at 635 nm and 1550 nm. For both the static and vibrated cases, each individual set of 10 frames was averaged to provide better SNR.

Table 2. Laser diode modal noise test procedure

Test	Wavelength	Neutral Density Filter	Frame integration time (low gain)	Static or Vibrated
1	1550 nm	7×10^{-4}	600 µs	Static
2	1550 nm	7×10^{-4}	600 µs	Vibrated
3	635 nm	10^{-2}	300,000 µs	Static
4	635 nm	10^{-2}	300,000 µs	Vibrated
5	635 nm	10^{-2}	30,000 µs	N/A (single mode)

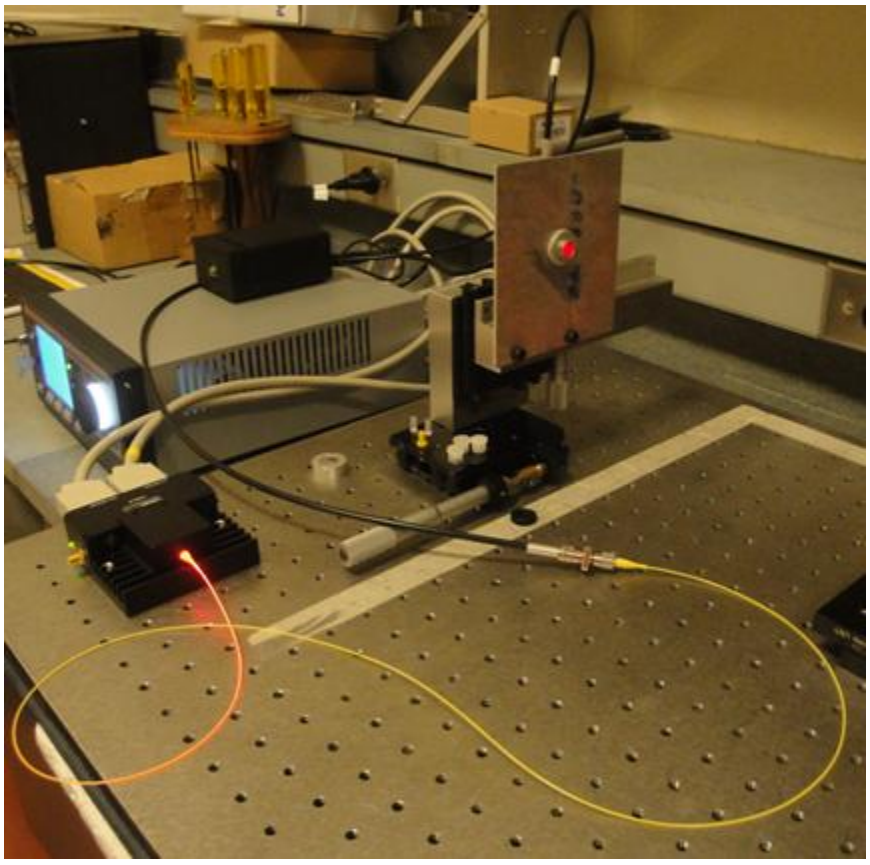

Fig. 5. 635 nm static test

4. RESULTS AND ANALYSIS

Fig. 6 displays the results from the 635 nm single mode fiber test, with the image centroid marked by a red plus sign. As expected, the 635 nm laser diode produced a virtually noiseless Gaussian profile of the single mode fiber's sole fundamental mode. This serves as a comparison to the static and vibrated multimode fiber modal noise results.

(a) (b)

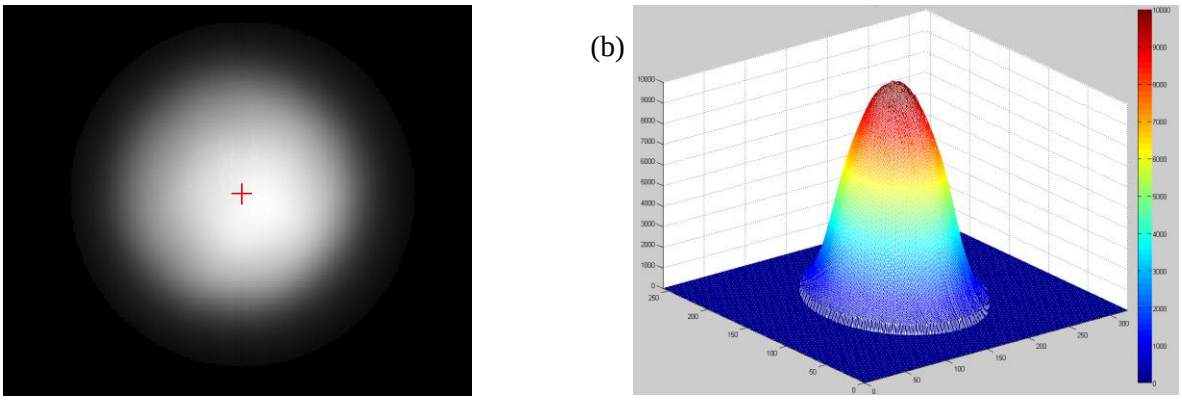

Fig. 6. Single mode fiber test – (a) 635 nm image, (b) 635 nm 3D intensity plot

Fig. 7 features the results of the 635 nm laser diode static and vibrated tests. For the static case, large mode patterns can be seen across the face of the fiber and are readily apparent in the 3D intensity plot. These modal patterns change between all 10 sets of 635 nm static frames, indicating the mixing of the modes with each flick of the fiber between individual sets. However, vibration of the multimode fiber has largely removed the modal patterns in Fig. 7 (c) and (d). Not only is there less modal noise present, but the noise that remains has smaller amplitude fluctuations.

(a) (c)

(b) (d)

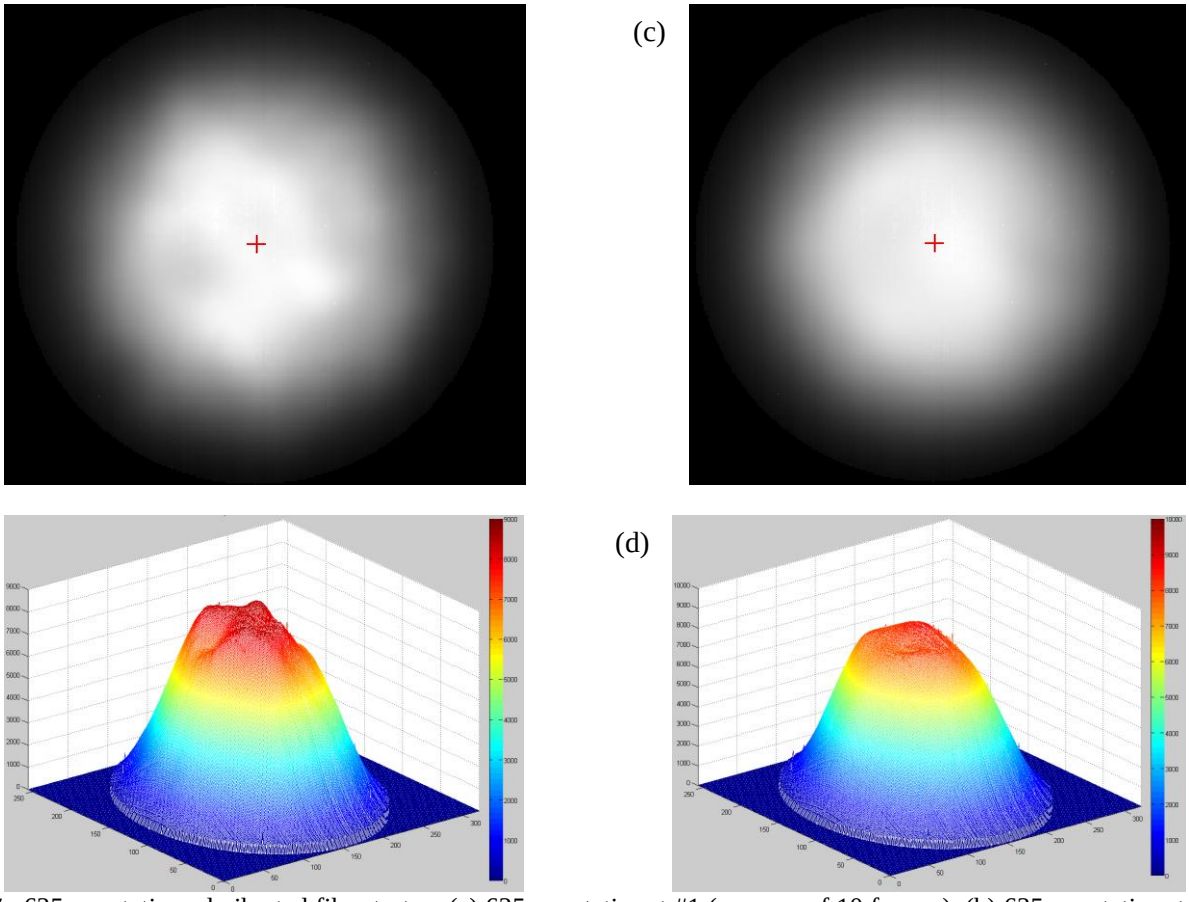

Fig. 7. 635 nm static and vibrated fiber tests – (a) 635 nm static set #1 (average of 10 frames), (b) 635 nm static set #1 3D intensity plot, (c) 635 nm vibrated frames (average of 100 frames), (d) 635 nm vibrated frames 3D intensity plot

Fig. 8 shows the 1550 nm laser diode static and vibrated fiber tests. Many more modes are readily visible in the fiber output speckle pattern and with a much greater range of intensities than the 635 nm case. Once again,

vibrating the multimode fiber has the effect of reducing the modal noise and smoothing over the intensities, though modal noise clearly remains. Reviewing the statistics from these averaged frames sheds more light on the differences between the 635 nm and 1550 nm static and vibrated test results.

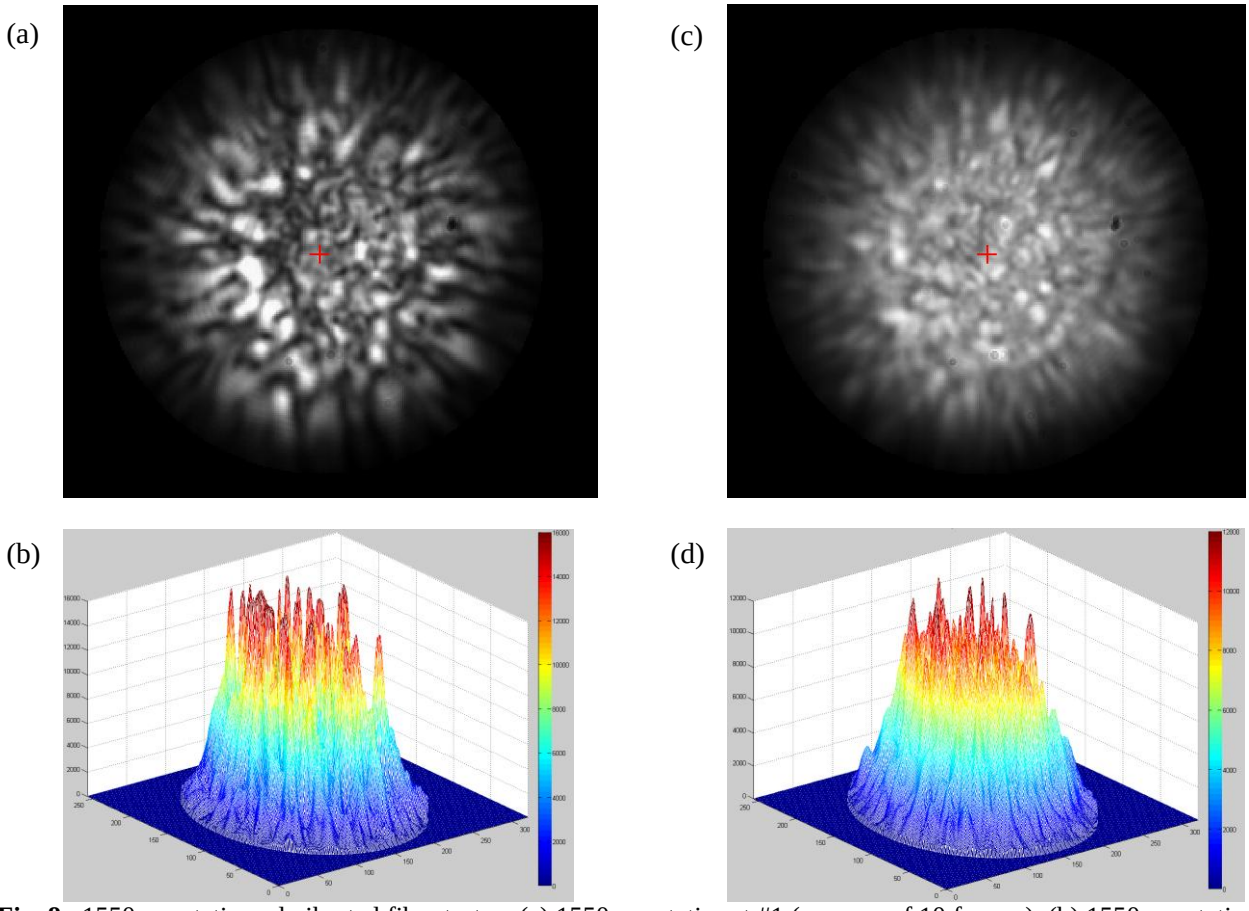

Fig. 8. 1550 nm static and vibrated fiber tests – (a) 1550 nm static set #1 (average of 10 frames), (b) 1550 nm static set #1 3D intensity plot, (c) 1550 nm vibrated frames (average of 100 frames), (d) 1550 nm vibrated frames 3D intensity plot

Tables 3 and 4 contain the average pixel value, standard deviation, and variances for the 635 nm and 1550 nm tests, respectively. The standard deviations and variances are similar between the static and vibrated sets in the 635 nm case, though the vibrated numbers are slightly lower. This is in agreement with the reduction in modal noise witnessed in the averaged frames and the corresponding 3D intensity plots. Furthermore, the majority of the individual averaged vibrated sets have standard deviations and variances below that of the average of all 100 vibrated frames. For the 1550 nm case, the standard deviations and variances for the vibrated sets are more significantly lower than the static sets, indicating a reduction in modal noise. The average of all 100 vibrated frames has a lower standard deviation and variance than any of the individual vibrated sets.

Table 3. 635 nm test statistics

	Average Pixel Value	Standard Deviation	Variance
Static – Set #1	3710	2634	6.9381e+06
Static – Set #2	3707	2617	6.8464e+06
Static – Set #3	3708	2629	6.9132e+06
Static – Set #4	3791	2697	7.2715e+06
Static – Set #5	3723	2655	7.0498e+06
Static – Set #6	3797	2714	7.3643e+06
Static – Set #7	3765	2697	7.2714e+06
Static – Set #8	3728	2642	6.9784e+06
Static – Set #9	3698	2577	6.6432e+06
Static – Set #10	3770	2662	7.0862e+06
Vibrated – Set #1	3761	2643	6.9831e+06
Vibrated – Set #2	3749	2640	6.9673e+06
Vibrated – Set #3	3760	2668	7.1185e+06
Vibrated – Set #4	3737	2638	6.9587e+06
Vibrated – Set #5	3748	2643	6.9869e+06
Vibrated – Set #6	3731	2616	6.8443e+06
Vibrated – Set #7	3738	2641	6.9750e+06
Vibrated – Set #8	3736	2614	6.8336e+06
Vibrated – Set #9	3745	2631	6.9214e+06
Vibrated – Set #10	3736	2642	6.9773e+06
Vibrated – All sets	3744	2636	6.9489e+06

Table 4. 1550 nm test statistics

	Average Pixel Value	Standard Deviation	Variance
Static – Set #1	4261	3496	1.2224e+07
Static – Set #2	4319	3717	1.3817e+07
Static – Set #3	4162	3442	1.1846e+07
Static – Set #4	4389	3855	1.4860e+07
Static – Set #5	4159	3446	1.1873e+07
Static – Set #6	4243	3736	1.3955e+07
Static – Set #7	4267	3668	1.3454e+07
Static – Set #8	4178	3508	1.2307e+07
Static – Set #9	4240	3498	1.2236e+07
Static – Set #10	4266	3586	1.2855e+07
Vibrated – Set #1	4260	3201	1.0245e+07
Vibrated – Set #2	4165	3116	9.7117e+06
Vibrated – Set #3	4092	3409	1.1622e+07
Vibrated – Set #4	4147	2992	8.9494e+06
Vibrated – Set #5	4132	3051	9.3085e+06
Vibrated – Set #6	4037	3218	1.0355e+07
Vibrated – Set #7	4164	3156	9.9629e+06
Vibrated – Set #8	4252	3030	9.1815e+06
Vibrated – Set #9	4106	3265	1.0657e+07
Vibrated – Set #10	4199	2976	8.8583e+06
Vibrated – All sets	4155	2905	8.4415e+06

Averaged frames, 3D intensity plots, and statistics provide evidence of modal noise reduction, but 2D FFT and spatial frequency power spectrum plots provide a clearer picture of this effect from a purely frequency standpoint. Fig. 9 contains log-scaled plots (centered on the origin) of 2D FFT magnitude for the 635 nm and 1550 nm static set #1 and vibrated cases. Fig. 10 displays the 2D rotationally averaged spatial frequency power spectrum plots for all 4 test cases, with normalized power and frequency axes. From Figs. 9 and 10, a very slight reduction in low spatial

frequencies can be discerned going from the 635 nm static set #1 to the vibrated case. This verifies the modal reduction seen in the 2D and 3D visualizations of the frames in Fig. 7, along with the statistics provided in Table 3. The reduction of low spatial frequencies is more readily seen in the 1550 nm 2D FFT and power spectrum plots. Though it is visually clear that modal noise was reduced for the 1550 nm case in the 2D and 3D frames in Fig. 8 and statistically in Table 4, Fig. 9 and 10 demonstrates that it is the low spatial frequency noise that is reduced the most.

These tests prove that modal noise was reduced by vibration in both cases, but longer integration times obviously need to be tested to fully characterize modal noise reduction for the visible and NIR. The integration times for these individual static and vibrated frames ranges from 0.6–300 ms, but integration times on the order of 1 second will need to be tested to more closely match Pathfinder's much longer exposure time.

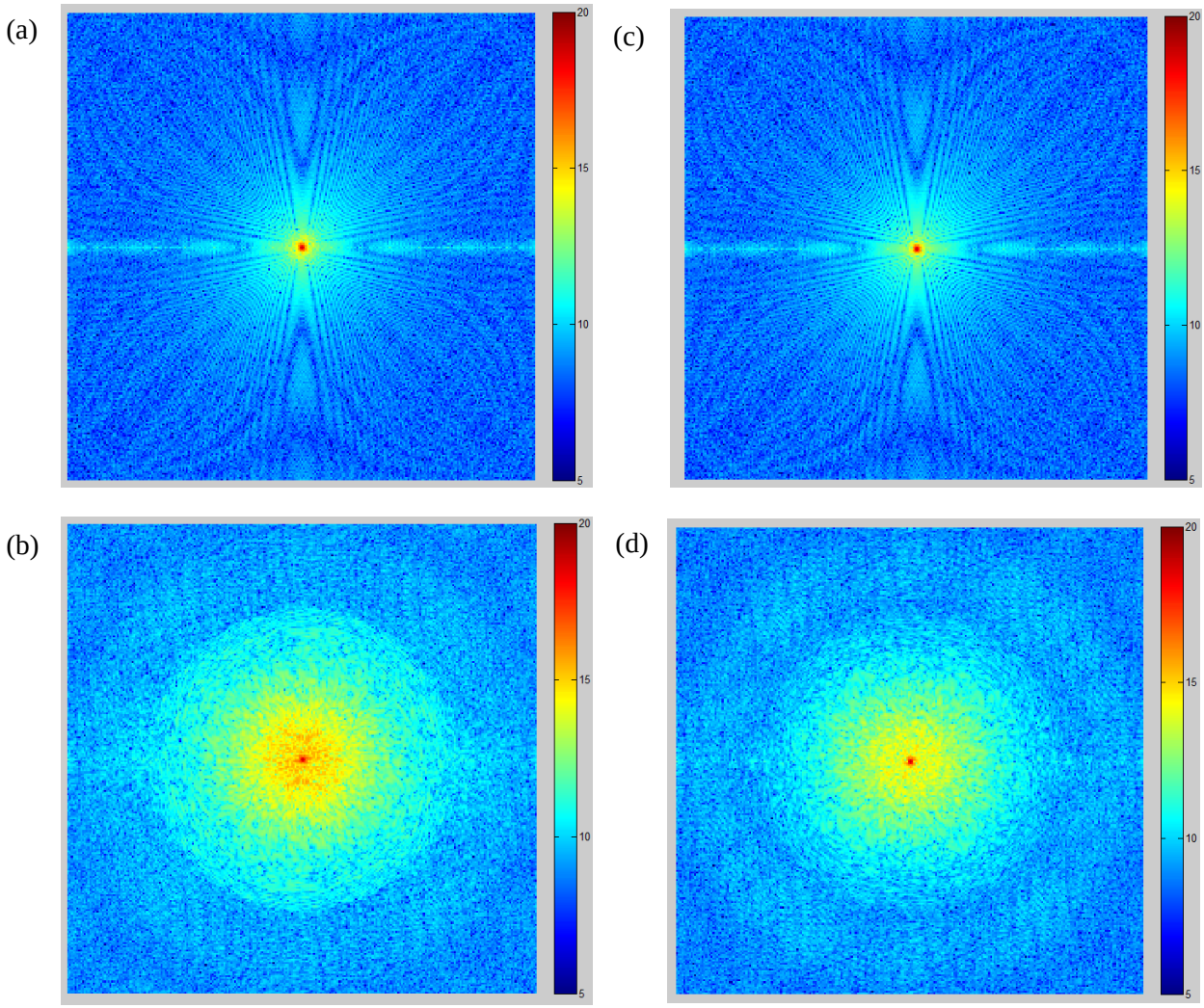

Fig. 9. 2D FFTs – (a) 635 nm static set #1 (average of 10 frames), (b) 1550 nm static set #1 (average of 10 frames), (c) 635 nm vibrated frames (average of 100 frames), (d) 1550 nm vibrated frames (average of 100 frames)

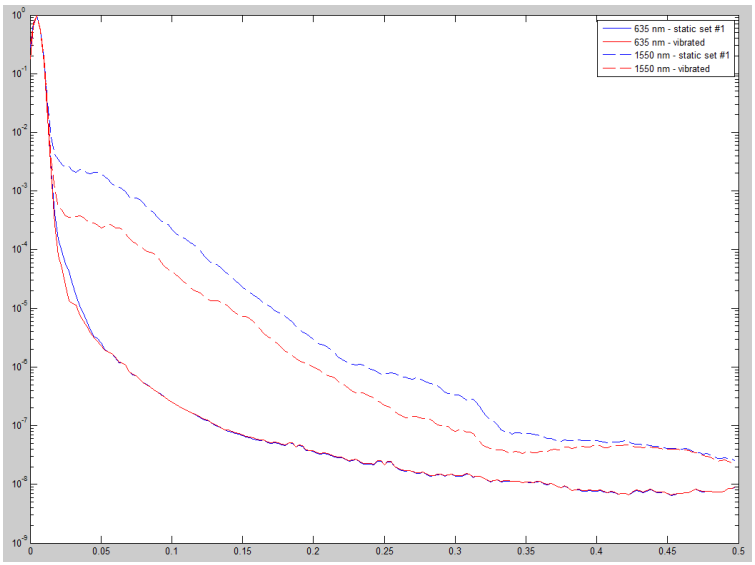

Fig. 10. 2D spatial frequency power spectrum – (solid blue line) 635 nm static set #1 (average of 10 frames), (solid red line) 635 nm vibrated (average of 10 frames), (dashed blue line) 1550 nm static set #1 (average of 10 frames), (dashed red line) 1550 nm vibrated frames (average of 100 frames)

5. CONCLUSIONS

These preliminary laser diode tests are a precursor for more extensive tests to follow in characterizing and mitigating modal noise in Penn State's Pathfinder spectrograph. It was seen that modal noise, particularly of low spatial frequencies, was reduced by vibrating the multimode fiber. This effect was more pronounced at 1550 nm than for 635 nm, though clearly longer integration times that more closely match exposure times for Pathfinder need to be tested. Visual wavelength laser diodes need to be tested with a camera more responsive at their wavelengths. These future tests will characterize FRD, modal noise, and scrambling techniques at various wavelengths in the visible and NIR. Pathfinder is a prototype for Pathfinder II, a facility-class, cooled, high-resolution NIR spectrograph capable of high-precision radial-velocity measurements of Earth-mass planets orbiting mid- to late-type M dwarfs. The lessons learned through this research will contribute to the efforts in enabling Pathfinder II to achieve < 5 m/s precision in the NIR

6. ACKNOWLEDGEMENTS

This research is supported by NASA grant NNX09AB34G, L. Ramsey, PI. I would like to thank Dr. Larry Ramsey, my master's thesis advisor, and Dr. Suvrath Mahadevan, for their invaluable advice and expertise in helping me carry out these experiments.

7. REFERENCES

[1] Schneider, J., "The Extrasolar Planets Encyclopaedia," http://exoplanet.eu/catalog.ph, 2011.

[2] Ramsey, Larry et al., "The Pathfinder Testbed: Exploring Techniques for Achieving Precision Radial Velocities in the Near-Infrared," Proceedings of the SPIE, Vol. 7735, 2010.

[3] Kasting, James et al., "Habitable Zones around Main Sequence Stars," ICARUS, Vol. 101, 108-128, 1993.

[4] Corbett, J. and Allington-Smith, J., "Fibre modal noise in astronomical spectrophotometry," Proceedings of the SPIE, Vol. 6269, 2006.

[5] Barden, Samuel., "Review of Fiber-Optic Properties for Astronomical Spectroscopy," ASP Conference Series, Vol. 152, 1998.

[6] Lo Curto, Gaspare et al., "Along the path towards extremely precise radial velocity measurements",2010.

[7] Lemke, U. et al., "Characterising modal noise in fibre-coupled spectrographs for astronomy," Proceedings of the SPIE, Vol. 7739, 2010.